Original Research

Meninges act as a gate for EEG & DDG: only MHz frequencies can reflect from 14 layers, defining consciousness – a clinical study

Pushpendra Singh[1], Sarika Katiyar[2,$], Saifullah Tipu[2,$], Shanthi Banishetty[3], Tanusree Dutta[3], Rupesh Ranjan[4], Stuart Hameroff[5], Anirban Bandyopadhyay[6,*]

[1]Sapiotectronics Lab, IKSMHA Centrer, Indian Institute of Technology Mandi, Kamand - Mandi, Himachal Pradesh, 175075 India
[2]Bhopal Memorial Hospital and Research Center (BMHRC), Department of Anaesthesia and Critical Care, Bhopal, 462024 India
[3]Indian Institute of Management (IIM), Organisational Behavior & Human Resources Management, Ranchi, Jharkhand, 834008 India
[4]Bhopal Memorial Hospital and Research Center (BMHRC), Department of Psychiatry, Bhopal, 462024 India
[5]Arizona Astrobiology Center, and Anesthesiology and Psychology, University of Arizona, Tucson, AZ, 85721 USA
[6]Materials and Nanoarchitectronics, MANA, National Institute for Materials Science (NIMS), Tsukuba, 305-0044 Japan

[$]Both authors contributed equally to this manuscript.

*Correspondence: anirban.bandyopadhyay@nims.go.jp and anirban.bandyo@gmail.com
DOI: https://doi.org/10.56280/1686004826

Received: 15 March 2025 Accepted: 21 March 2025 Online published: 30 March 2025

Abstract

Despite traditional EEG signals being affected by physical activities such as hand movements, facial expressions, and perspiration, they have been considered indicators of consciousness for over a century and a half. Low-frequency signals ranging from 1 Hz to 40 Hz are associated with human cognition, perception, and emotion. We challenge the 150-year belief that low-frequency neuron bursts are key to human consciousness; ions are diluted at 15 layers before reaching the EEG probe. We argue that MHz electromagnetic signals govern key computing in the brain. In our study of 40 patients undergoing anesthesia with propofol for gastroenteric conditions, we monitored transitions into and out of unconsciousness, comparing EEG signals with those from the DDG. MHz bursts are emitted from all over the brain's scalp only in unconscious states, as tracked by BIS, and disappear upon regaining consciousness. Strikingly, identical bursts appear in microtubule bundles of cultured hippocampal neurons only when a neuron fires; therefore, we attribute the MHz bursts observed in anesthetized patients to microtubule bundles in the neurons. We virtually created and simulated 15 layers between the scalp and the cortex, finding that ionic signals (in the range of Hz to kHz) are disrupted but still able to transmit. Meanwhile, MHz signals partially transmit and primarily reflect back deep inside the cortex, while GHz signals are largely attenuated at short distances. Collectively, the meninges form a 6–212 MHz gateway for critical brain signals from the cortex to the scalp, with a significant portion of the signal primarily reflecting back to the cortex. Anaesthesia may unlock this gate, allowing true MHz brain signals to leak until the meninges release transmitted anesthetic molecules. The one-to-one match between single-neuron bursts and those in the foreheads of unconscious patients suggests that the meninges gate's 14-channel pathway to the scalp and positioning of microtubules are the true neural correlates of consciousness.

Keywords: EEG, DDG, anaesthesia, cortex, scalp, meninges, consciousness, microtubules

1. Introduction

Recent studies have explored the effects and characteristics of electromagnetic radiation (EMR) from the brain. Kublanov et al. (2000) analyzed the time-and-frequency fluctuation intensity distributions of EMR from human brain structures, highlighting its relevance in monitoring cerebral circulation disorders. Wiginton et al. (2022) introduced a non-contact sensor capable of measuring the dynamic electromagnetic fields of the human brain, revealing distinct activity patterns during tasks and auditory stimulation. The electromagnetic signals were attributed to motor neurons (Brazdzionis, 2022). Furthermore, Bryukhovetskiy et al. (2020) proposed a theory suggesting that the human mind has a microwave electromagnetic nature, which implies that cognitive processes can be recorded and analyzed through the brain's electromagnetic activity, potentially leading to advancements in diagnostics and brain-computer interfaces. Despite numerous reports on low-power microwave radiation (femto-watt) from the scalp, no study has thoroughly examined how different brain components influence signal transmission. Our research investigates whether certain signals can pass through all layers-bones, cerebrospinal fluid, and blood vessels unhindered. By analyzing each layer from skin to cortex, we aim to determine if specific brain signals can truly leak through. To the best of our knowledge, no such study has been performed.

Journal of Multiscale Neuroscience

2. Materials and Methods

2.1 Theoretical simulation

We have created 15 layers of the brain structure as a square-shaped slice to its physical scale; we have put a probe similar to our experimental measurement on top of this slice. The external cylindrical hollow cover visible in Figure 3 is the ground part of the electrode, and the sharp needle is the positive electrode that captures the signals. The ground part protects the external signal from entering into the actual probe that measures the signal from the scalp. Also, an external electromagnetic signals, AC or EEG-like DC, could get absorbed into the water layer of the skin, so when the circular edge of the electrode touches tightly into the skin, the external surface, that is the conduction of AC and DC signals from outside the external skin surface is sent to the ground. Only the signal from within the circular boundary created by the ground electrode enters the sharp needle that takes the signal from skin to the spectrum analyzer. We have replicated this geometric feature in the theoretical simulator to accurately simulate the experimental conditions.

One could see 15 layers as follows, 1. Skin, 2. Dense connecting tissue, 3. Aponeurosis, 4. Loose connecting tissue, 5. Periosteum, 6. Outer cortical bone, 7. Middle diploe bone, 8. Inner cortical bone, 9. Dura matter, 10. Pia matter, 11. Arachnoid matter, 12. Bridging neurons, 13. Superior Sagittal Sinus, 14. Sub-arachnoid space. 15. Cortical columns with helical microtubule nanowire. We have carried out an extensive literature search to find the critical dielectric parameters of all these 15 layers. In reality, there are multiple different components in these layers. Therefore, there should not be one but a set of many dielectric constants for each of the 15 layers. Our simulator built-in Python currently takes an average value for each layer, but we can vary that significantly to adjust and find how signals could transmit inwards and outwards. We have provisions to adjust the dielectric constant, permittivity, and permeability with respect to the thickness of each layer. Additionally, we could assign electromagnetic coupling between layers.

Literature is rich in dc or low-frequency ionic conductivity of each layer. So, we have simply put the values from the literature, as various researchers have routinely measured these values. We have created a Python program to simulate the transmission of ionic potential through 14 layers. Note that ionic transport interacts with each layer's local ions, while electromagnetic frequencies in the MHz range will interact with the dipoles of each layer. The physics of interaction is very different for two types of systems. GHz signals, on the other hand, interact with much smaller dipoles. We select suitable components for signals ranging from Hz to GHz and utilize them as electromagnetic resonators. Eventually, we found a suitable frequency range, where the signal could transmit through 14 layers.

For microtubules and neurons, we have been measuring dielectric properties for over a decade, resulting in a comprehensive database of resonance frequencies. So, we have included a microtubule bundle-like structure in the cortical column. For all other layers, we conducted an extensive literature search. We will provide an overview of the 14 layers in the discussion section.

2.2 Study Design and Participants

This observational study was conducted on 40 patients undergoing elective surgical procedures under general anesthesia. Participants were recruited across diverse age groups and health backgrounds to ensure demographic variability. All patients provided informed consent prior to inclusion in the study, after receiving a comprehensive explanation of the experimental protocol and the noninvasive signal monitoring technique. The MHz detection probe was vertically positioned on the forehead, ensuring that the neutral, concave section of the sensor maintained full skin contact for optimal signal acquisition.

2.3 Monitoring Systems and Equipment

Two monitoring systems operated concurrently throughout the procedure:

1. **Standard Monitoring**: BIS values were recorded using the Aspect A-2000 BIS Monitor (BIS 2000 XP).
2. **Experimental MHz System**: High-frequency electromagnetic bursts were detected using a GW Instek GSP-730 Spectrum Analyzer (frequency range: 15 kHz to 3 GHz; dimensions: 105 mm × 153 mm × 296 mm). An SMA connector served as the MHz probe and was applied directly to the patient's forehead. To avoid artifacts and preserve data integrity, no filters, amplifiers, or averaging techniques were applied. All MHz signals were recorded as raw, unprocessed data.

Multiple spectrum analyzers were used to eliminate device-specific bias.

2.4 Anesthesia Protocol

Anesthesia was induced and maintained using standard pharmacological protocols. The following agents and dosages were administered:

- **Induction**: Propofol at 2–2.5 mg/kg bolus, followed by maintenance at 100–150 mcg/kg/min, in accordance with published protocols (Parikh & Mehta, 2012).
- **Analgesia**: Fentanyl at 2–3 mcg/kg/hr.
- **Neuromuscular Blockade**: Rocuronium at 1–1.2 mg/kg bolus for intubation, followed by maintenance dosing at 0.5 mg/kg.
- **Reversal Agents**: Glycopyrrolate (0.01 mg/kg) and neostigmine (0.05 mg/kg) were administered upon observation of spontaneous respiratory efforts.
- **Antiemetic**: Ondansetron (100 mcg/kg) administered pre-extubation.

Throughout surgery, intermittent propofol boluses and inhalational anesthetics were administered to maintain BIS scores between 40 and 50. Minimum alveolar concentration (MAC) values were maintained within the range of 0.2–1, and oxygen saturation (SpO_2) was kept above 94% in all patients.

2.5 Procedure and Data Collection

Both the BIS and MHz monitoring systems were activated prior to anesthesia induction and continued through post-extubation until full recovery of consciousness. Data were captured at five critical phases: pre-induction, post-induction, maintenance, extubation, and full recovery.

MHz signal bursts, particularly in the 6–26 MHz range, were dynamically recorded over the forehead region (Singh et al. (2023, 2024). These bursts, morphologically similar to neuronal spike activity, emerged only during the anesthetized state and were absent in both pre-induction and post-recovery phases. Correlative analyses were performed between BIS values and MHz signal patterns, with particular attention to the induction and emergence periods.

Notably, in several patients, MHz bursts persisted in specific forehead regions even after BIS values returned to 100, indicating that MHz-based monitoring may provide a more sensitive index for the return of consciousness than conventional BIS. These findings suggest that MHz signal tracking may serve as a complementary or superior modality for preventing intraoperative awareness and assessing anesthetic depth.

3. Results and Discussions

3.1 Comparison between microtubule burst inside a neuron and scalp reading of a human patient under anesthesia

We present the data from our previous measurement on the neurofilament bundle of a single neuron, as recorded using a patch clamp (Figure 4a of Ghosh et al., 2016), in greater detail in **Figures 1** and **2**. Side by side, we have plotted the MHz burst reading from a patient that appears only in the presence of anesthesia, in **Figure 2b**. Though the negative part of MHz burst that we see in the filamentary bundle during a nerve impulse in **Figure 2a** is missing in case of anesthetized patient in **Figure 2b**, we clearly find that pulse width, pulse height and the gap between pulses are identical. Striking similarity of neuron signal and brain signal.

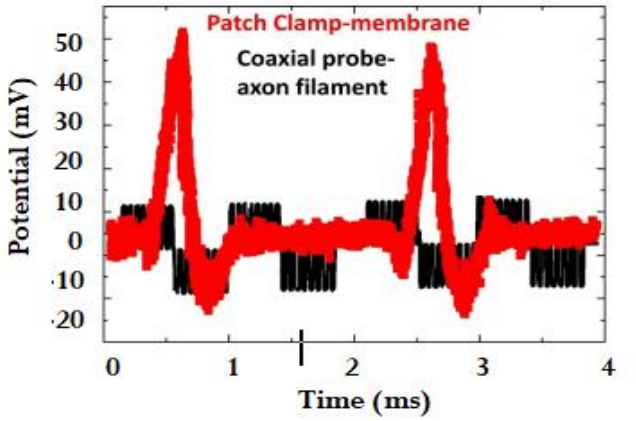

Figure 1. *Hippocampal neuron membrane potential was measured using a patch clamp on a culture plate, and simultaneously, an atomic sharp needle was inserted deep inside the axon of that neuron. The experimental details and explanation of the study can be found in our previous paper (Figure 4a of Ghosh et al., 2016); we had previously published this plot in a different format. The red plot depicts the* nerve impulse measured by a Patch Clamp and black plot is the signal generated by filament assembly, simultaneously.

We measured single filament using a coaxial probe; probably that's why the intensity was 5mV. Because in the case of patients, we find its 10mV, just doubled. We do not currently have any explanation for this increment; however, emission could be the collective effect of microtubule bundles inside an axon. Note that a neuron has unidirectionally oriented microtubules inside, and collectively, they can generate a significant amount of electromagnetic communication with other neuron's microtubule bundles.

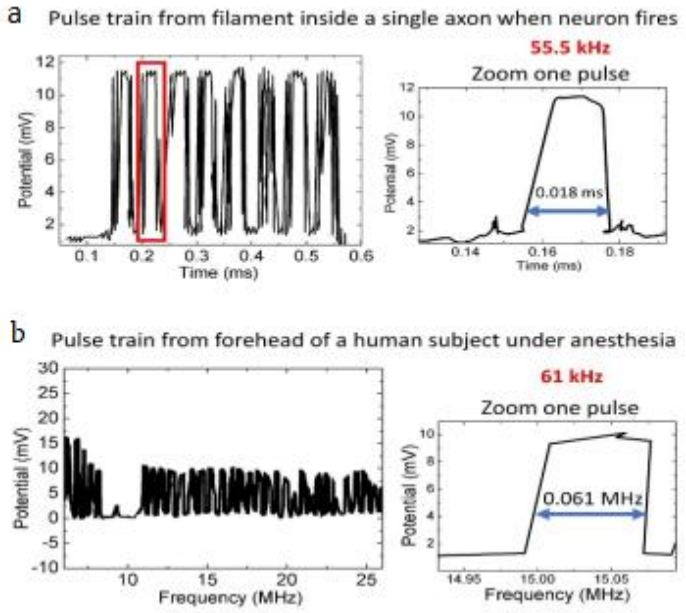

Figure 2. *We have zoomed in twice on the filamentary bursts observed in Figure 1. Using the SMA probe, which we touched on the forehead of a patient under anesthesia with a BIS value of around 40-50, we found a burst in the spectrum analyzer's range of 6MHz to 26MHz. We have zoomed one pulse to its right. We find that the pulse widths are the same for both cases. More than 20 different culture plates we studied in 5 separate batches, we always observed the 55-60kHz bursts from neurofilaments. For all 40 patients studied, we observed 58-64kHz bursts from the forehead of anesthetic patients.*

3.2 Theoretical simulation to confirm that the ionic signals cannot be responsible for consciousness. It is an output of a deeper conscious process

3.2.1. Simulation 1: Ionic signal inside the brain will get messed up by 14 layers

We have created a virtual device, a piece of cortex-to-scalp representation, in the CST software, as shown in **Figure 3**. In this Maxwell's equation solver, we need to provide the input dielectric properties of all materials and their dimensions. While discussing, we will detail how we gathered those values and solved Maxwell's equations to understand the dielectric uniqueness of the structure. Conductivity differences between different layers (see **Table 1**) are such that any ionic transmission cannot sustain its potential as it passes through the ionic barriers. Estimating the effect of conductivity gradient when ionic/nerve potential moves from cortex to scalp:

- **Stratified Medium**: 15 layers with distinct DC conductivity (σ_1–σ_{15}) and homogeneous within each layer.
- **Propagation Mode**: Transverse Magnetic (TM) waves, as VLF primarily uses TM modes in Earth-ionosphere waveguides
- **Frequency Range**: Near-DC to 30 kHz (quasi-static regime).

Fraction of signal transmitted between layers n and n+1, we have used Transmission Coefficient $T = \left\{\{2Z\_\{n+1\}\}\{Z\_n + Z\_\{n+1\}\}\right\}$, while attenuation constant was derived by

$$\alpha = \omega \sqrt{\frac{\mu\epsilon}{2}\left(\sqrt{1+\left(\frac{\sigma}{\omega\epsilon}\right)^2}-1\right)}$$

Layer-by-Layer Propagation

1 Boundary Conditions:

- Electric field continuity: $E_t^{(n)} = E_t^{(n+1)}$
- Current density continuity: $\sigma_n E_n = \sigma_{n+1} E_{n+1}$

2 Cumulative Attenuation:

$$A_{\text{total}} = \sum_{i=1}^{15} \alpha_i d_i \text{ (dB)}, \; \alpha_i \propto \frac{1}{\sqrt{\sigma_i}}$$

- Higher conductivity layers reduce attenuation (e.g., seawater $\sigma \approx 4\,\text{S/m}$ vs. dry soil $\sigma \approx 0.001\,\text{S/m}^3$.

Table 1. Conductivity and general dielectric properties of different layers between cortical columns and the skin

Tissue/Component	Conductivity (S/m)	Dielectric Properties	Frequency/ Type	Reference	Notes/Additional Information
Cerebrospinal Fluid (CSF)	1.79 - 1.81	High dielectric constant (~109 at 10 Hz)	AC, low-frequency	Latikka & Eskola, 2018	Highest in vivo conductivity in human tissues
Scalp	0.41	Moderate dielectric constant	AC/DC, low-frequency	McCann et al., 2019	Important for EEG source localization
Whole Skull	~0.02	Low dielectric constant	AC/DC, low-frequency	McCann et al., 2019	Highly resistive, impacts EEG accuracy
Gray Matter	0.47	Relatively high dielectric constant	AC/DC, low-frequency	McCann et al., 2019	Crucial for modeling electrical brain activity
White Matter	0.22	Intermediate dielectric constant	AC/DC, low-frequency	McCann et al., 2019	Affects propagation of electromagnetic signals
Brain-to-Skull Conductivity Ratio (BSCR)	Aug-80	High variability	Low-frequency EEG	Acar et al., 2016	Crucial parameter influencing EEG modeling accuracy
Meninges Adjusted CSF	~0.85 (emulated effect)	Adjusted dielectric properties	AC/DC, low-frequency	Jiang et al., 2020	Improved EEG modeling accuracy when included
Human Skin	0.0002 - 0.5	Dielectric constant (~1000 at Hz range)	10 Hz - 10 MHz	Baumann et al., 1997; Fernández-Corazza et al., 2016	High variability due to moisture, temperature, conditions
Blood	0.7	High dielectric constant (~5250 at 100 Hz)	AC, low-frequency	Gabriel et al., 1996	Affects electromagnetic field penetration
Fat	0.02	Low dielectric constant	AC/DC, low-frequency	Gabriel et al., 1996	Provides insulation, impacts electromagnetic modeling
Bone (cortical)	0.02 - 0.06	Low dielectric constant	AC/DC, low-frequency	Gabriel et al., 1996	Similar conductivity to skull, influences EEG signal clarity
Muscle	0.35 - 0.7	High dielectric constant (~8000 at 100 Hz)	AC, low-frequency	Gabriel et al., 1996	Conductivity depends on fiber direction, hydration, frequency
Electromagnetic Resonance Frequency (Microtubules)		MHz range (~6-26 MHz)	Megahertz frequencies	Our experimental data	Observed experimentally under anesthesia (dodecanogram)

- Phase Shift:

$$\phi_{\text{total}} = \sum_{i=1}^{15} \beta_i d_i,\ \beta_i = \omega\sqrt{\mu\epsilon_i}$$

Path Loss Estimation from layer 1 to layer 15, destroying true brain signal if at all it is ionic

$$L_{\text{total}} = 32.4 + 20\log_{10}(f_{\text{MHz}}) + 20\log_{10}(d_{\text{km}}) + \sum_{i=1}^{15} A_i$$

- Dominated by conductivity-weighted attenuation $A_i \propto 1/\sqrt{\sigma_i}$.

We have used the following theory to find that whether it is inside the brain or outside, more than 3 barriers with 3 different conductivities, ionic signal cannot transmit until MHz modulation is added. This is why we argue the brain needs MHz. Note that MHz triggering generated 50-60kHz bursts, this frequency domain is also several orders higher than EEG signal.

The electrical DC or low-frequency conductivity of human tissues varies significantly, which impacts the characterization and modeling of electromagnetic sources. Cerebrospinal fluid (CSF) has the highest conductivity, measured in vivo at 1.79-1.81 S/m (Latikka & Eskola, 2018). Scalp conductivity is approximately 0.41 S/m, while the whole skull conductivity is around 0.02 S/m (McCann et al., 2019). The conductivities of gray and white matter are estimated at 0.47 S/m and 0.22 S/m, respectively (McCann et al., 2019). The brain-to-skull conductivity ratio (BSCR) varies widely, with estimates ranging from 8 to 80 (Acar et al., 2016). Accurate modeling of head tissues is crucial for EEG source localization, as skull conductivity misestimation can potentially cause errors of up to 3 cm (Acar et al., 2016). Recent studies suggest that including meninges in models or adjusting CSF conductivity to 0.85 S/m to emulate meningeal effects can improve accuracy (Jiang et al., 2020). Conductivity values are influenced by factors such as measurement methods, temperature, and individual variations (Baumann et al., 1997; Fernández-Corazza et al., 2016).

Cerebrospinal fluid: Research on the electromagnetic properties of cerebrospinal fluid (CSF) has revealed its distinctive dielectric behavior at microwave frequencies, which can be used to differentiate between normal and abnormal samples (Lonappan et al., 2006). These properties are influenced by factors such as glucose and protein levels, potentially aiding in early disease detection (Noetscher et al., 2012). CSF's dielectric parameters vary with temperature and frequency, which can be modeled using the Debye equation (Wang et al., 2024). High-resolution proton NMR spectroscopy has been utilized to identify metabolites in cerebrospinal fluid (CSF), demonstrating promise for diagnosing conditions such as bacterial meningitis and liver failure (Bell et al., 1987). Novel electromagnetic sensors have been developed for real-time monitoring of CSF components, such as lactate (Mason et al., 2013). Additionally, MRI-derived structural data of the brain has been used to simulate dielectric resonance, revealing characteristic electromagnetic field distributions in various brain components (Singh et al., 2018).

EEG signal is therefore mixed with ionic signals of all 15 layers, we have taken compounded effect in **Figure 4.**

Table 2 demonstrates that distinct anesthetic molecules generate unique rhythmic signatures, highlighting the absence of a singular, universal mechanism underlying consciousness. Identifying an invariant feature—independent of anesthetic type—is essential. While MHz signals offer promising insight into cognitive processes, pinpointing a definitive source remains challenging. Given the abundance of helical nanowires in neurofilaments and microfilaments, precise identification of their frequency contributions demands further high-resolution studies. Currently, microtubule bundles within axon cores emerge as the most probable candidates for mediating these MHz dynamics.

Table 2: Variations of EEG pattern with anesthesia

Anesthetic Type	Molecular Target	Dominant EEG Frequencies	Clinical EEG Pattern
Propofol	GABA_A	Alpha (8–13 Hz), Slow (0.5–4 Hz)	Frontal alpha coherence; burst suppression at high doses145
Isoflurane/Sevoflurane	GABA_A, NMDA	Theta (4–8 Hz), Alpha	Frontoparietal alpha-theta coherence; prolonged suppressions178
Ketamine	NMDA	Gamma (30–80 Hz)	Dissociative gamma oscillations; preserved low-frequency power8
Etomidate	GABA_A	Beta (13–30 Hz)	Beta activation with spindle-like waves; minimal slow oscillations3
Thiopental	GABA_A	Delta (0.5–4 Hz)	Rapid progression to burst suppression; suppressed alpha/beta26
Nitrous Oxide	NMDA	Mixed beta/gamma	Increased beta (13–30 Hz) with preserved consciousness; less delta

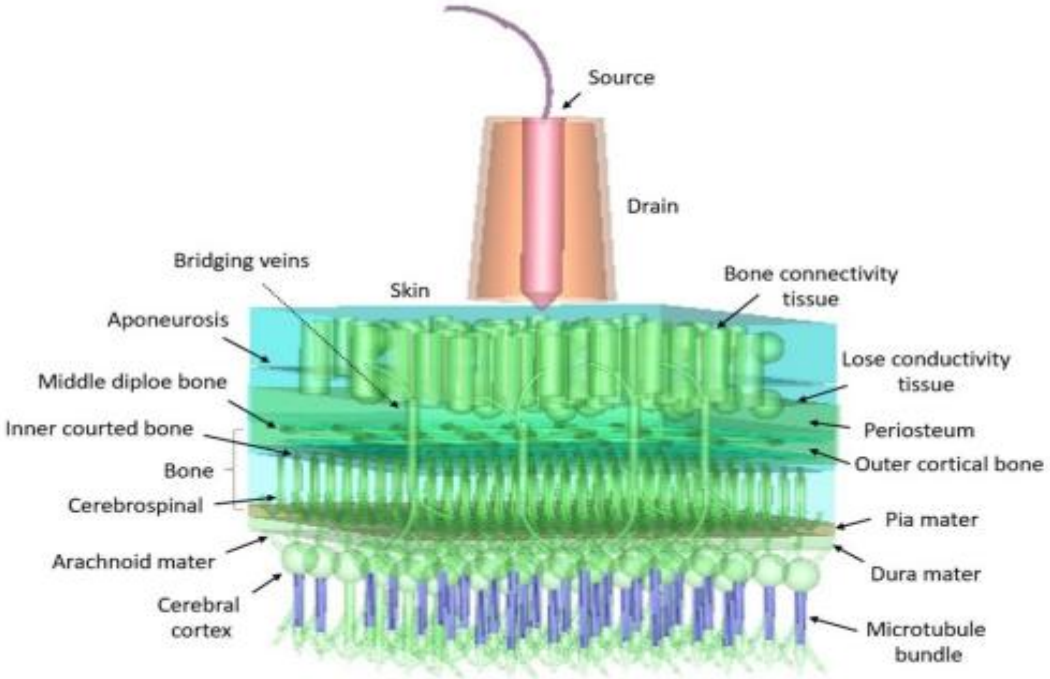

Figure 3. *In the Computational Science and Technology (CST) simulator, we recreated virtual hardware, as shown above, to simulate various types of signal transmission. We provide three tables Table 1, Table 2 and Table 3, compiled from different works of literature, the structural parameters already published, and we are still fine-tuning to replicate a real physical scenario, when a signal tries to enter inside the brain and when a signal emits from inside.*

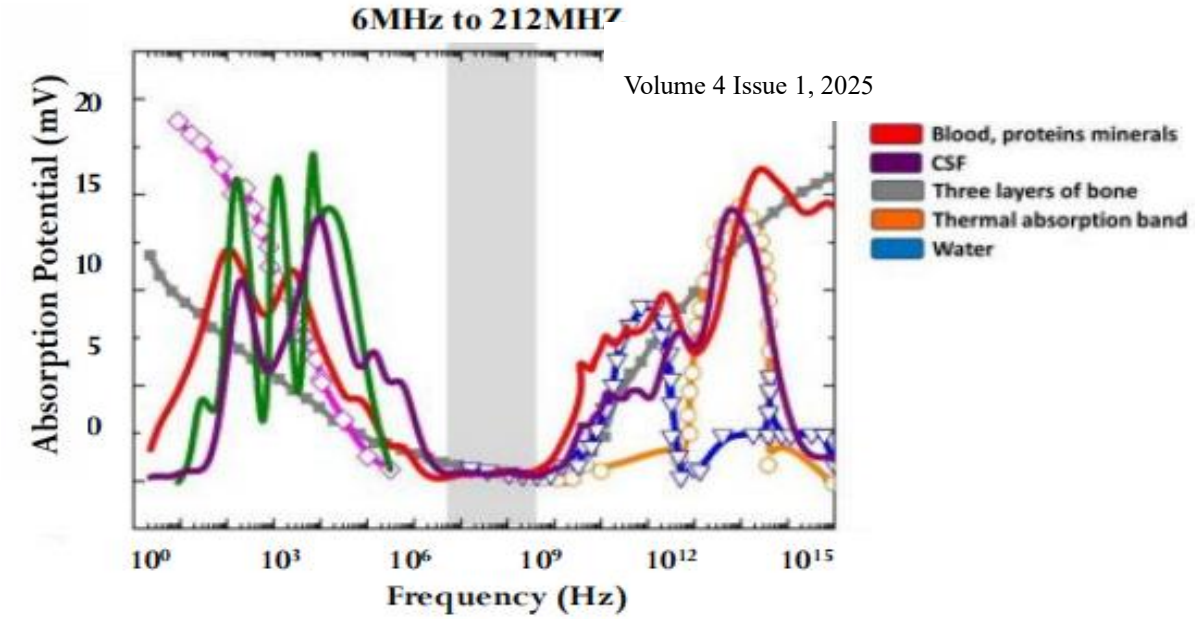

Figure 4. *This is a summary of all AC and DC simulations for 15 layers plotted together. Ions of other layers do not absorb low-frequency or ionic transmissions. However, there are significant sharp gradients in low-frequency conductivity among all 15 layers that disrupt the shape of potential; the effective resistance is high, and we have calculated as low-frequency absorption. Around THz, there is thermal absorption. As Hz and GHz signals are compromised for two distinct reasons, only MHz signals with minimal absorption can be partially emitted and largely reflected back (note that absorption, transmission, and reflection add up to 1).*

3.2.2 Simulation 2: Only MHz signal can reflect back

Human blood's and CSF's dielectric properties vary by frequency—cell membrane polarization dominates between 1-100 MHz, while above 1 GHz, water molecule motion in plasma becomes significant. The skull has small channels for blood vessels and nerves but doesn't significantly transmit electromagnetic signals. EEG technology, using multiple electrodes and signal processing, distinguishes deep brain activity from surface nerve signals. Brain neurons exhibit rhythmic firing, which is essential for cognition, unlike sensory nerves, which produce sharp, localized impulses. To confirm microtubule-generated megahertz signals, rigorous testing, shielding, and controlled comparisons are needed. Ionic solutions can transmit signals up to the MHz range, but impedance increases at higher frequencies. Blood, with a higher ion and protein content, may conduct AC signals more effectively than cerebrospinal fluid, which primarily consists of water, proteins, glucose, and electrolytes.

White matter reflects most incident power, with minimal absorption and shallow penetration. Low-grade gliomas exhibit optical properties similar to those of gray matter. Meningiomas and glioblastomas absorb significantly more than normal brain tissue.

Why do meninges behave abnormally compared to the other 14 layers?

The script computes Reflection (R) and Transmission (T) coefficients for each interface using:

$$R = \left|\frac{Z_2 - Z_1}{Z_2 + Z_1}\right|^2$$
$$T = 1 - R$$

where $Z = \sqrt{\mu/\varepsilon}$ for each layer.

A. Boundary Conditions for MHz Signals

At MHz frequencies $(1 - 100\text{MHz})$:

- Wave impedance mismatch dominates reflection/transmission behavior.
- Intrinsic impedance of tissue layer n :

$$Z_n = \sqrt{\frac{j\omega\mu}{\sigma_n + j\omega\epsilon_n}}$$

where $\omega = 2\pi f, \epsilon_\pi = \epsilon_0\epsilon_{r,n}$, and σ_n is the layer's conductivity.

B. Reflection Coefficient

The reflection coefficient at the dura-CSF interface:

$$\Gamma = \frac{Z_{\text{CSF}} - Z_{\text{Dura}}}{Z_{\text{CSF}} + Z_{\text{Dura}}}$$

Transmission coefficient: $T = 1 + \Gamma$.

A. Dura → CSF Interface

- Impedance mismatch: $Z_{\text{Dura}} \gg Z_{\text{GSF}}$ due to CSF's higher σ.
- Reflection coefficient:

$$\Gamma_{\text{Dura/CSF}} = \frac{1.6(1-j) - 6.3(1-j)}{1.6(1-j) + 6.3(1-j)} \approx -0.59$$

- Reflection magnitude: $|\Gamma| \approx 59\%$
- Phase inversion: Negative Γ indicates a 180° phase shift.

B. Partial Transmission

- Transmitted power: $|T|^2 = 1 - |\Gamma|^2 \approx 1 - 0.35 = 65\%$.
- Attenuation in CSF:

$$\alpha_{\text{GSF}} = \frac{\sigma_{\text{GSF}}}{2}\sqrt{\frac{\mu}{\epsilon_{\text{GSF}}}}$$

≈ 1.2 Np/m (negligible over 1 − 2 mm thickness).

Signal Pathways

A. Reflected Wave {59%} :

- Returns to the brain through pia-arachnoid-dura layers.
- Secondary reflection at brain-CSF interface ($\Gamma_{\text{Erain /CSF}} \approx +0.7$) reinforces signal confinement.

B. Transmitted Wave (41%):

- Penetrates CSF with minimal loss (skin depth $\delta_{\text{CSF}} \approx 2.3$ m at 10 MHz).
- Subsequent reflection at CSF-brain interface (Γ_{CSF} Brain $\approx +0.7$) redirects 70% back toward the meninges.

We have summarized the results in **Figure 4** and **Figure 5**.

The reflection coefficient as a function of frequency shows that GHz-range frequencies are attenuated locally; kHz and Hz signals, however, transmit through, due to changes in conductivity across the 14 layers. We have summarized the values of various dielectric parameters in the **Table 3**. Note that every layer has a complex structure, and the smaller the dimension, the larger the value of the dielectric constant. We have found that the composition of meninges is unique.

3.2.3 Simulation 3: Theoretical origin of triplet in conscious patients and experimental verification

Signals cannot enter from outside, because of DC conductivity difference, nature has uniquely built conductivity differences such that anything enters from outside would be diminished. However, signals can come out of the 14 layers from inside. This is not true that high frequency signals transmit through our body, extreme fluidity of the skin with insulating layers make it a perfect absorber of environmental signal and convert them into ionic flow. This is the reason; EEG signals are mixed with environmental noise.

4. Meninges: The gateway to the scalp

The meninges, composed of three layers (dura mater, arachnoid mater, and pia mater), contain neurons, glial cells, and an extensive vascular network. Meninges harbor embryonically derived radial glia-like progenitors that migrate into the cerebral cortex and differentiate into functional neurons, such as Satb2+ neurons in cortical layers II-IV. These cells exhibit neurogenic potential and integrate into cortical circuits (Bifari, 2017). The meninges are in close contact with

Table 3. Dielectric properties of all 15 layers

Component	ε_r	ε (F/m)	μ (H/m)	Z (Ω)	f (Hz)	R (Interface)	T (Interface)
Air (initial)	1	8.85×10^{-12}	1.257×10^{-6}	377	-	-	-
1. Skin	45	4.0×10^{-10}	1.257×10^{-6}	56.0	2.24×10^{10}	-0.74 (Air-Skin)	0.26 (Air-Skin)
2. Dense Conn. Tissue	55	4.85×10^{-10}	1.257×10^{-6}	50.9	2.02×10^{10}	-0.05 (1-2)	0.95 (1-2)
3. Aponeurosis	55	4.85×10^{-10}	1.257×10^{-6}	50.9	2.02×10^{10}	0.00 (2-3)	1.00 (2-3)
4. Loose Conn. Tissue	65	5.75×10^{-10}	1.257×10^{-6}	46.7	1.86×10^{10}	-0.04 (3-4)	0.96 (3-4)
5. Periosteum	55	4.85×10^{-10}	1.257×10^{-6}	50.9	2.02×10^{10}	0.04 (4-5)	1.04 (4-5)
6. Outer Cortical Bone	15	1.35×10^{-10}	1.257×10^{-6}	96.5	3.87×10^{10}	0.35 (5-6)	1.35 (5-6)
7. Middle Diploë Bone	10	0.85×10^{-10}	1.257×10^{-6}	121.7	4.74×10^{10}	0.12 (6-7)	1.12 (6-7)
8. Inner Cortical Bone	15	1.35×10^{-10}	1.257×10^{-6}	96.5	3.87×10^{10}	-0.12 (7-8)	0.88 (7-8)
9. Dura Mater	625,000	5.53×10^{-6}	1.257×10^{-6}	0.0151	6.00×10^{6}	-0.9997 (8-9)	0.0003 (8-9)
10. Pia Mater	2,250,000	1.99×10^{-5}	1.257×10^{-6}	0.0079	1.00×10^{8}	-0.31 (9-10)	0.69 (9-10)
11. Arachnoid Mater	500,625	4.43×10^{-6}	1.257×10^{-6}	0.0168	2.12×10^{8}	0.36 (10-11)	1.36 (10-11)
12. Bridging Veins	70	6.2×10^{-10}	1.257×10^{-6}	45.0	1.79×10^{10}	-0.04 (11-12)	0.96 (11-12)
13. Superior Sag. Sinus	70	6.2×10^{-10}	1.257×10^{-6}	45.0	1.79×10^{10}	0.00 (12-13)	1.00 (12-13)
14. Sub-Arachnoid Space	80	7.1×10^{-10}	1.257×10^{-6}	42.1	1.68×10^{10}	-0.03 (13-14)	0.97 (13-14)
15. Cortical Columns	60	5.3×10^{-10}	1.257×10^{-6}	48.7	1.94×10^{10}	0.07 (14-15)	1.07 (14-15)
Air (final)	1	8.85×10^{-12}	1.257×10^{-6}	377	-	0.80 (15-Air)	1.80 (15-Air)

cerebrospinal fluid (CSF), which plays a role in distributing anesthetic molecules within the central nervous system (CNS). Lipid-soluble anesthetics can diffuse through the meninges, potentially interacting with neuronal or glial cells near the brain surface (Abd-Elsayed, 2024). If meninges act as a temporary reservoir for lipid-soluble anesthetics, they might influence the timing of unconsciousness and recovery. **Figure 5** shows that three layers of meninges, acting independently, significantly alter the way the SMA probe measures filamentary bundle emission as part of our high-frequency characterization.

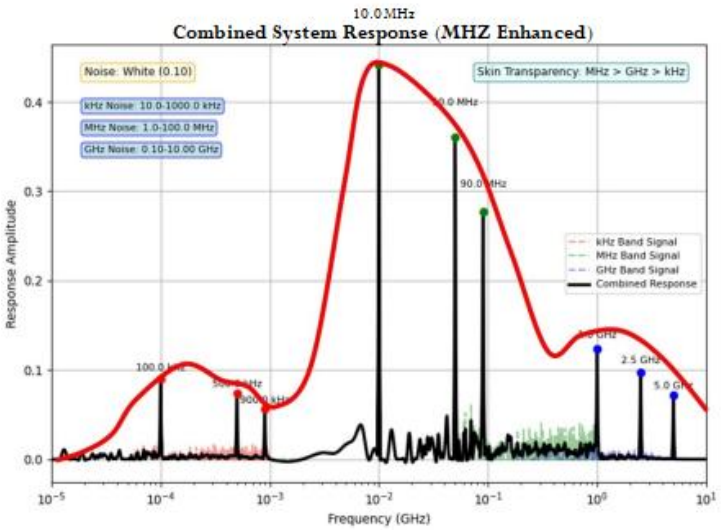

Figure 5. *Another simulation of transmitted signal from 15th layers helical structure, i.e. microtubule to the skin crossing the 14 layers in between. The black line is the vibrational spectrum of the microtubule in the cortical column's neuron and red line is the average output of the bundle's vibrations, this is also the triplet (earlier triplet was observed in neurons and microtubules, Saxena, K., (2020)) we observe in the awake persons forehead experimentally.*

The dura mater contains blood vessels that could facilitate the absorption of anesthetic molecules into systemic circulation. Redistribution of these molecules could theoretically contribute to regaining consciousness as their concentration declines in the brain. Lipid-soluble anesthetics, such as propofol, can cross biological membranes, including the meningeal layers, due to their physicochemical properties (Decloux, 2020). This raises the possibility that meninges temporarily retain anesthetics before releasing them back into circulation or CSF.

We argue that meninges play a crucial role in governing the shape of the DC potential distribution and AC signal that we observe on the scalp.

How do we ensure that Dodecanogram, DDG (Dutta, & Bandyopadhyay, 2024), here with SMA probe connected to spectrum analyzer), does not collect environmental signals from the skin, if EEG absorbs them, then DDG too should absorb?

Of course, environmental signals absorbed in the water layer of the skin should have a chance to be collected; however, like EEG, we have found ways to detect changes. We have a separate ground cap covering the electrode. This cap acts like a cavity. The cavity acts like a resonator, amplifying the signal.

The proposed theory involves using an SMA coaxial cable as a shielded cavity to capture brain-derived AC signals while mitigating environmental noise. Here is a synthesis of how this setup could function based on coaxial cable principles and neural signal acquisition:

5. Theory of Operation

5.1 Coaxial Shielding for Noise Rejection

- **Outer Ground Cap (2.5 mm diameter)**:
  The SMA's outer conductor (shield) acts as a Faraday cage, isolating the central signal-carrying needle from external electromagnetic interference (EMI). When in contact with the skin, it establishes a low-impedance reference ground, diverting environmental noise away from the neural signal path.
- *Key Mechanism*: The skin's conductivity (~0.1–1 S/m) allows the shield to dissipate capacitive/inductive noise via the body's natural grounding.
- *Frequency Range*: Effective for brain signals (0.5–100 Hz EEG) but optimized for SMA's design range (DC–18 GHz).

5.2 Central Sharp Needle (Signal Conductor):

A tapered, high-conductivity (e.g., silver-plated copper) needle penetrates the skin to interface with extracellular ionic

currents from neuronal activity. Its sharpness minimizes contact impedance and localized tissue damage.

5.3 Cavity Resonance and Signal Coupling

- **Skin-Cable Interface as a Cavity**:
  The dielectric properties of skin (ε_r ≈ 40–50 at 1 kHz) and SMA's PTFE insulator (ε_r = 2.1) create a mismatched transmission line. This mismatch reduces signal reflection at the skin-cable interface.
- **Signal Propagation**:
  Neural AC signals (μV–mV range) induce currents in the needle, which travel along the central conductor. The coaxial structure's characteristic impedance (~50 Ω) minimizes standing waves caused by impedance mismatches.

5.4 Noise Elimination Mechanisms

- **Common-Mode Rejection**:
  Environmental noise (e.g., 50/60 Hz mains, MHz radio wave, GHz mobile signal) couples equally to the shield and needle, allowing differential amplifiers to subtract noise via common-mode rejection (CMRR > 100 dB).
- **Skin-Electrode Interface**:
  The shield's large surface area (2.5 mm diameter) stabilizes the reference potential, while the needle's small contact area maximizes signal sensitivity.

Coaxial Transmission Line Model

A coaxial cable supports the propagation of TEM (Transverse Electromagnetic) waves. The electric (E) and magnetic (H) fields in cylindrical coordinates (r, ϕ, z) are:

$$E_r = \frac{V(z)}{r \ln(b/a)},\ H_\phi = \frac{I(z)}{2\pi r}$$

where $a =$ inner conductor radius (needle), $b =$ outer conductor radius (shield), $V(z) =$ voltage, and $I(z) =$ current.

The telegrapher's equations describe voltage/current propagation:

$$\frac{\partial V}{\partial z} = -(R + j\omega L)I,\ \frac{\partial I}{\partial z} = -(G + j\omega C)V$$

- R : Conductor resistance per unit length
- L : Inductance per unit length $\left\{L = \frac{\mu}{2\pi} \ln(b/a)\right\}$
- G : Dielectric conductance per unit length
- C : Capacitance per unit length $\left(C = \frac{2\pi\epsilon}{\ln(b/a)}\right)$

2 Neural Signal Coupling

The central needle detects extracellular ionic currents from neurons. The induced voltage V_{signal} is proportional to the current density J :

$$V_{\text{signal}} = \int_{\text{needle}} \frac{J \cdot \hat{r}}{4\pi\sigma r^2} dV$$

- σ: Conductivity of brain tissue ($\sim 0.1 - 1$ S/m)
- r: Distance from neural source to needle

3 Shielding Effectiveness (SE)

The outer shield attenuates environmental noise via:

$$\text{SE(dB)} = 20\log_{10}\left(\frac{E_{\text{unshielded}}}{E_{\text{shielded}}}\right) = A + R + M$$

- Absorption Loss (A):

$$A = 8.686 \cdot t\sqrt{\pi f \mu \sigma_{\text{shield}}}$$

$t =$ shield thickness, $f =$ frequency, $\mu =$ permeability, $\sigma_{\text{shield}} =$ shield conductivity.

- Reflection Loss (R):

$$R = 168 - 10\log_{10}\left(\frac{\mu_r f}{\sigma_{\text{shield}}}\right)$$

- Multiple Reflections (M): Negligible for thick shields.

For a 2.5 mm Ag-plated Cu shield $\{t = 0.1\text{ mm}, \sigma_{\text{shield}} = 6.3 \times 10^7\text{ S/m}\}$, SE at 60 Hz :

$$A \approx 120\text{ dB},\ R \approx 100\text{ dB} \Longrightarrow \text{Total SE} \approx 220\text{ dB}$$

4 Signal-to-Noise Ratio (SNR)

SNR depends on neural signal power (P_{signal}) and noise power (P_{noise}):

$$\mathrm{SNR} = \frac{P_{\text{signal}}}{P_{\text{noise}}} = \frac{|V_{\text{signal}}|^2}{k_B T \Delta f + |V_{\text{noise}}|^2}$$

- $k_B T \Delta f$:Thermal noise (Johnson-Nyquist }
- $V_{\text{noise:}}$ Residual environmental noise after shielding
- Cutoff Frequency

The SMA cable's cutoff frequency for non-TEM modes (TE/TM) is:

$$f_c = \frac{c}{\pi(a+b)\sqrt{\epsilon_r}}$$

For $a = 0.1$ mm (needle), $b = 1.25$ mm (shield), $\epsilon_r = 2.1$ (PTFE):

$$f_c \approx 31.8\text{GHz (far above EEG's } 0.5 - 100 \text{ Hz)}$$

This ensures TEM dominance and minimal dispersion.

Table 4: Simulation results of MA Probe that measures MHz busts

Shield Conductivity	$_{\text{shield}} = 6.3 \times 10^7$ /m(Cu)	Maximizes absorption loss
Skin Impedance	$\approx 1 - 10\text{k}\Omega$ at 1 Hz	Requires conductive gel for impedance matching
Needle Radius	$a < 10\mu$ m	Minimizes invasiveness while maintaining signal sensitivity

This framework demonstrates **Table 4** that SMA coaxial cables can theoretically capture neural signals while rejecting noise via shielding and impedance matching. Experimental validation would require testing SNR and biocompatibility *in vivo*.

6. Deep brain components responsible for consciousness

The evidence overwhelmingly links anesthetic-induced unconsciousness to direct neural circuit modulation (e.g., thalamocortical suppression, delta-phase coupling), and awakening to a conscious state could be reflected in the activation of the thalamocortical pathway.

6.1 Deep Brain Nuclei Activation

Local field potentials (LFPs) from the thalamus and basal ganglia show synchronized slow oscillations (0.5–4 Hz) during anesthesia, which dissipate as consciousness returns. Subcortical deep brain nuclei are involved in the recovery of general anesthesia, and provide clues for solving the mystery of consciousness (Ongoing Clinical trial, Analysis of Deep Brain Nuclei LFP and Cortical EEG Signals During the Recovery From General Anesthesia; Shanghai Jiao Tong University; ClinicalTrials.gov ID NCT06400901; Sponsor Ruijin Hospital; Information provided by Xin Ma, MD, Ruijin Hospital (Responsible Party); Last Update Posted 2024-05-13).

Phase-Amplitude Coupling: Sevoflurane anesthesia induces delta-phase restriction of higher-frequency oscillations (8–30 Hz) in the cortex, directly observed via ECoG (Chamadia 2019). Authors argue that extracranial mechanisms are there. **Microvascular Correlations**: Anesthetics like isoflurane amplify cortical blood volume (CBV) oscillations associated with neural activity, as demonstrated through imaging during invasive experiments. **Thalamocortical Integration**: The thalamus acts as a relay hub for sensory and cortical signals. While it is essential for integrating cortical-subcortical communication, consciousness arises from thalamocortical networks, not solely from the thalamus. Propofol disrupts thalamocortical "core-matrix" architecture, shifting functional geometry toward unimodal (sensory/motor) dominance and away from transmodal (higher-order) integration (Huang, 2024). **Cortical Independence**: Slow oscillations (0.1–1 Hz) can persist in isolated cortical slices without thalamic input (Flores, 2017).

We are not arguing here that the meninges are responsible for consciousness; we argue that among 14 layers, this layer, the meninges, is best equipped for credible signal transmission outside the brain.

6.2 Should the brain use a Hz signal or a MHz signal?

These higher frequencies are less likely to leak through the brain tissue and more likely to reflect within the brain, allowing for more controlled and localized processing. This could help maintain the integrity of the computational signals and prevent unwanted leakage. By leveraging these higher frequencies, the brain can potentially enhance signal confinement, ensuring that its internal processes remain more stable and accurate. Comparing Hz and kHz signals, using higher frequencies such as MHz or GHz could indeed be beneficial in the context of artificial brain engineering.

6.3 Dielectric properties of 15 layers from scalp to cortical columns in the cortex

We have already discussed the above simulations for all 15 years and have extensively utilized the resulting values. Here is **Table 5** and the review of literature pertaining to dimensions of different components.

Layer 1: Skin: The dielectric constant and conductivity of skin vary inversely as it is exposed to electromagnetic signals after MHz electromagnetic irradiation (radio waves), particularly at low frequencies (Tamura et al., 1994). Measurements of the epidermis and dermis separately show that their dielectric properties differ from those of whole skin, especially at frequencies above 20 GHz (Sasaki et al., 2014); therefore, we simulated skin at frequencies below 10 GHz. The penetration depth of electromagnetic fields from open-ended coaxial probes varies with frequency, with higher frequencies (>100 MHz) penetrating deeper layers and lower frequencies (<10 MHz) mainly affecting superficial structures (Alanen et al., 1999). Between 10 MHz and 100 MHz, specific components resonate, resulting in a narrow signal transmission band. Dielectric properties of tissues are influenced by factors such as temperature, ion concentration, and dilution (Davarcioğlu, 2011).

Layer 2, dense connecting tissue: (Sadleir & Gabriel, 2021). Recent research has uncovered intriguing connections between the brain cortex and the scalp. The mechanical or electrical stimulation of the trigeminal nerves innervates scalp acupoints and provides a neurologic pathway (*trigeminal nerve–meninges–cerebrospinal fluid–contacting neurons–brain*) for scalp-cortex functional regulation (WangShuya et al., 2017). We have modeled this pathway to find its potential to act as an electromagnetic signal transmission route.

Layer 6, 7, 8: Bone: Different parts of the brain bones modulate electromagnetic signals differently. The parietal bone allows for higher transmission and less phase distortion compared to the frontal and occipital regions, with transmission being negatively correlated to skull thickness. A three-layer model incorporating bone absorption has been proposed to estimate maximum pressure transmission through the skull for frequencies between 100 kHz and 1.5 MHz (Attali et al., 2022). This model illustrates that transmission decreases with frequency and bone thickness, exhibiting peaks at multiples of half-wavelength. For microwave absorption, resonance effects have been observed in theoretical models of the skull (Joines & Spiegel, 1974).

The dielectric properties of bones are crucial for understanding their interaction with electromagnetic waves, particularly in medical applications (Amin et al., 2019). These properties vary in frequency and are influenced by bone mineral density, which may be potentially useful for osteoporosis diagnosis (Amin et al., 2018). The human skull exhibits resonance absorption of microwaves, with absorption patterns differing between homogeneous and inhomogeneous models (Joines & Spiegel, 1974). Bone's dielectric properties are related to its water content and composition (Foster & Schwan, 1989; Gabriel et al., 1996). The acoustic characteristics of the skull, including absorption and scattering, influence ultrasound imaging (White et al., 1978). The acoustic properties of the skull bone, such as propagation velo-

Table 5: Structural details of various layers between the cortex and the skin

Region	Layer	Thickness Range	Typical Thickness	Additional Structural Details
Scalp	Skin	0.5–2.5 mm	~1.5 mm	Collagen-rich, contains sweat glands, hair follicles, and sensory nerves.
	Connective tissue	1–4 mm	~2 mm	Dense fibrous tissue, highly vascularized, provides nourishment.
	Aponeurosis (Galea)	0.5–1 mm	~0.5 mm	Fibrous layer connecting frontalis and occipitalis muscles.
	Loose areolar tissue	1–3 mm	~2 mm	Allows scalp mobility, vascular, potential space for infections.
	Pericranium	~0.5 mm	~0.5 mm	Thin connective tissue layer covering skull bones, osteogenic function.
Skull (Calvaria)	Outer cortical bone	1–2 mm	~1.5 mm	Dense bone providing mechanical protection and structure.
	Diploë (spongy bone)	2–8 mm	~4 mm	Porous bone, vascularized, aids in shock absorption.
	Inner cortical bone	0.5–1.5 mm	~1 mm	Dense bone closely adherent to dura mater.
Meninges	Dura mater	0.5–1.5 mm	~1 mm	Tough fibrous layer, rich in collagen, forms venous sinuses.
	Arachnoid mater	0.05–0.2 mm	~0.1 mm	Delicate, avascular membrane facilitating CSF circulation.
	Pia mater	0.01–0.05 mm	~0.02 mm	Very thin, highly vascular membrane, closely adherent to brain cortex.
Venous Sinuses/Subarachnoid	Superior sagittal sinus	2–10 mm (width varies)	~5 mm	Major venous sinus within dura mater, drains cerebral blood.
	Subarachnoid space (CSF-filled)	1–5 mm	~3 mm	CSF-filled, cushions the brain, circulates nutrients and waste.
Cerebral Cortex Region	Falx cerebri	0.86–0.96 mm	0.91 ± 0.05 mm	Thick dural fold separating cerebral hemispheres, houses venous channels.

city and absorption coefficient, have been experimentally measured (Martin & McElhaney, 1971). Understanding these properties is vital for various medical applications, including cancer treatment and bone healing stimulation (Pethig, 1984). However, variations in reported data suggest the need for further research in this area.

Bridging veins: Bridging veins play a crucial role in draining blood from the cerebral cortex to the superior sagittal sinus (SSS) (Famaey et al., 2015). These veins have a complex structure and mechanical behavior, with distinct morphological changes at the SSS junction (Famaey et al., 2015). The cortical-SSS junction features a myoendothelial "sphincter" that may regulate cerebral venous hemodynamics (Vignes et al., 2007). Bridging veins are part of a transcephalic DC circuit, potentially transmitting signals from the cortex to the scalp through the skull (Cowen et al., 1967). This pathway of least resistance links cortex and scalp, with the cortex likely being the main generator of transcephalic DC potentials (Cowen et al., 1967). An abundance of collagen and elastin in tunica adventitia covers the outside of the vein. Collagen's triplet helices make them good carriers of triplet of triplet resonance signals absorbed and emitted by microtubules.

Layer 9, 10, 11, Meninges: Recent research has explored the electromagnetic properties of meninges and their impact on brain stimulation techniques. Studies have shown that meninges significantly affect the electric fields in transcranial electrical stimulation (TES), increasing cortical field strength by approximately 30% (Weise et al., 2022). Modeling the cerebrospinal fluid (CSF) conductivity at 0.85 S/m, rather than the conventional 1.65 S/m, better emulates the presence of meninges and improves accuracy in TES models (Jiang et al., 2020). Meninges also influence the optical properties of brain tissue, affecting laser penetration in neurosurgery (Eggert & Blazek, 1987). Furthermore, the meninges play crucial roles in brain development, homeostasis, and response to injury (Decimo et al., 2012). They may even harbor stem cells with the potential for neural differentiation. Interestingly, electromagnetic fields generated by neurons have been found to influence neuronal processes and network dynamics (Scholkmann, 2015), with the local geomagnetic field affecting calcium ion efflux from brain tissue (Blackman et al., 1985).

Cortical column: The neocortex is organized into layers and columns, with neurons in vertical columns sharing similar response properties and connections (Goodhill & Carreira-Perpiñán, 2002; Mountcastle, 1957). Cortical columns consist of diverse neuron types, including excitatory projection neurons and inhibitory interneurons, each with distinct morphological, electrophysiological, and molecular characteristics (Tremblay et al., 2016; Amitai & Connors, 1995). These neurons form complex circuits that process sensory information and generate motor output (Wells, 2005; Kaas, 2010). The composition and properties of neurons within cortical columns vary across cortical areas and species, reflecting functional specializations (Jones & Rakic, 2010). Synapses between neurons exhibit plasticity, allowing for adaptive changes in network function (Jones, 1981). Understanding the cellular and synaptic relationships within cortical columns is crucial for elucidating normal brain function and identifying potential pathological changes (Jones & Rakic, 2010).

7. Conclusion

The human brain primarily functions using low-frequency signals, as detected in EEG measurements. However, there is evidence that structures like microtubules may operate at higher frequencies, potentially in the megahertz (MHz) range. These higher-frequency processes could contribute to more complex and fine-tuned brain functions. The overall complexity of the brain likely involves a combination of both low-frequency and high-frequency processes. While low-frequency signals are predominantly used for broader functions, high-frequency components could also play a vital role in specific areas of brain activity.

References

Abd-Elsayed, A., Abdallah, R.T. & Villatoro-Lopez,J. (2014) Meninges. In, Alaa Abd-Elsayed (Ed.), *Basic Anesthesia Review*. Oxford Academic, New York.

Acar, Z., Acar, C. & Makeig, S. (2016) Simultaneous head tissue conductivity and EEG source location estimation. *NeuroImage* **124**, 168-180.

Alanen, E., Lahtinen,T. & Nuutinen, J. (1999) Penetration of electromagnetic fields of an open-ended coaxial probe between 1 MHz and 1 GHz in dielectric skin measurements. *Physics in Medicine and Biology* **44**, N169–N176.

Amin, B., Elahi, M. A., Shahzad, A., Porter, E. & O'Halloran, M. (2019) A review of the dielectric properties of the bone for low frequency medical technologies. *Biomedical Engineering and Physics Express* **5**, 022001.

Amin, B., Elahi, M. A., Shahzad, A., Porter, E., McDermott, B. & O'Halloran, M. (2018) Dielectric properties of bones for the monitoring of osteoporosis. *Medical and Biological Engineering and Computing* **57**, 1-13.

Amitai, Y. & Connors, B. W. (1995) Intrinsic physiology and morphology of single neurons in neocortex. In, Jones, E.G., Diamond, I.T. (Eds) *The Barrel Cortex of Rodents*. Springer Nature, New York.

Attali, D., Tiennot, T., Schafer, M., Fouragnan, E., Sallet, J. et al. (2022) Three-layer model with absorption for conservative estimation of the maximum acoustic transmission coefficient through the human skull for transcranial ultrasound stimulation. *Brain Stimulation* **16**, 48-55.

Baumann, S., Wozny, D. R., Kelly, S., & Meno, F. (1997) The electrical conductivity of human cerebrospinal fluid at body temperature. *IEEE Transactions on Biomedical Engineering* **44**, 220-223.

Bell, J. D., Brown, J. C., Sadler, P., Macleod, A., Sönksen, P. et.al. (1987) High resolution proton nuclear magnetic resonance studies of human cerebrospinal fluid. *Clinical Science* **72**, 563-570.

Bifari, F., Decimo, I., Pino, A., Llorens-Bobadilla, E., Zhao, S. *et al*. (2017) Neurogenic radial glia-like cells in meninges migrate and differentiate into functionally integrated neurons in the neonatal cortex. *Cell Stem Cell* **20**, 360-373.

Blackman, C. F., Benane, S., Rabinowitz, J., House, D. E. & Joines, W. T. (1985) A role for the magnetic field in the radiation-induced efflux of calcium ions from brain tissue in vitro. *Bioelectromagnetics* **6**, 327-337.

Brazdzionis, J., Wiginton, J., Patchana, T., Savla, P., Hung, J. et. al. (2022). Evaluating the intrinsic electromagnetic field generated by neurons from repetitive motor activities in humans with a non-contact non-invasive electromagnetic helmet. *Cureus*, **14**, e23006.

Bryukhovetskiy, A. S., Brusilovsky,L.I., Kozhin,S.P., Serafimovich, P.G., Nikonorov, A.V. et. al. (2020) Human mind has microwave electromagnetic nature and can be recorded and processed. *Progress in Brain Research* **258**, 439–463.

Chamadia, S., Pedemonte, J.C., Hahm, E.Y. et al. (2019) Delta oscillations phase limit neural activity during sevoflurane anesthesia. *Communications Biology* **2**, 415.

Dutta, T. & Bandyopadhyay, A. (2024) DDG, an electromagnetic version of EEG finds evidence of a self-operating mathematical universe (SOMU): When a human subject converses with an artificial brain. In, *Emotion, Cognition and Silent Communication: Unsolved Mysteries*. Studies in Rhythm Engineering. Springer, Singapore.

Davarcioğlu, B. (2011) *The Dielectric Properties of Human Body Tissues at Electromagnetic Wave Frequencies*. SCISPAGE.

Decimo, I., Fumagalli, G., Berton, V., Krampera, M. & Bifari, F. (2012) Meninges: from protective membrane to stem cell niche. *American Journal of Stem Cells* **1**, 92-105.

Decloux, D. & Ouanounou, A. (2020) Local anaesthesia in dentistry: a review. *International Dental Journal* **71**, 87–95.

Eggert, H. & Blazek, V. (1987) Optical properties of human brain tissue, meninges, and brain tumors in the spectral range of 200 to 900 nm. *Neurosurgery* **21,** 459-464.

Famaey, N., Cui, Z. Y., Musigazi, G. U., Ivens, J., Depreitere, B. et. al. (2015) Structural and mechanical characterisation of bridging veins: A review. *Journal of The Mechanical Behavior of Biomedical Materials* **41**, 222-240.

Fernández-Corazza, M., Turovets, S., Govyadinov, P. A., Muravchik, C. & Tucker, D. (2016) Effects of head model inaccuracies on regional scalp and skull conductivity estimation using real EIT measurements. *Springer Proceedings* **54**, 5-8.

Flores, F.J., Hartnack, K.E., Fath,A.B., Kim,S-E., Wilson, M.A. et al. (2017) Thalamocortical synchronization during induction and emergence from propofol-induced unconsciousness. *Proceedings of the National Academy of Sciences (USA)* **114**, E6660-E6668,

Foster, K. & Schwan, H. (1989) Dielectric properties of tissues and biological materials: a critical review. *Critical Reviews in Biomedical Engineering* **17**, 25-104.

Gabriel, C., Gabriel, S. & Corthout, E. (1996) The dielectric properties of biological tissues: I. Literature survey. *Physics in Medicine and Biology* **41**, 2231.

Gabriel, C., Peyman, A. & Grant, E. (2009) Electrical conductivity of tissue at frequencies below 1 MHz. *Physics in Medicine and Biology* **54**, 4863.

Goodhill, G. & Carreira-Perpiñán, M. A. (2002) Cortical Columns. In, Lynn Nadel (Ed.), *Encyclopedia of Cognitive Science*. Macmillan, New York.

Ghosh, S., Sahu, S., Agrawal, L., Shiga, T. & Bandyopadhyay, A. (2016) Inventing a co-axial atomic resolution patch clamp to study a single resonating protein complex and ultra-low power communication deep inside a living neuron cell. *Journal of Integrative Neuroscience*, **15**, 403-433.

Huang, Z., Mashour, G.A. & Hudetz, A.G. (2024) Propofol disrupts the functional core-matrix architecture of the thalamus in humans. *Nature Communications* **15**, 7496.

Jiang, J., Truong, D., Esmaeilpour, Z., Huang, Y., Badran, B. & Bikson, M. (2020) Enhanced tES and tDCS computational models by meninges emulation. *Journal of Neural Engineering* **17**, 016027.

Joines, W. & Spiegel, R. (1974) Resonance Absorption of Microwaves by the Human Skull. *IEEE Transactions on Biomedical Engineering* **1**, 46–48.

Jones, D. G. (1981) *Neurons and Synapses,* in: Studies in Biology, 5: 1-60. London: Edward Arnold Punlishing.

Jones, E. & Rakic, P. (2010) Radial columns in cortical architecture: It is the composition that counts. *Cerebral Cortex* **20**, 2261–2264.

Kaas, J.H. (2010) Cortical Circuits: consistency and variability across cortical areas and species. In, *Dynamic Coordination in the Brain: From Neurons to Mind.* Eds, C. von der Malsburg, W. A. Phillips, & W. Singer), MIT Press, Cambridge, MA.

Kublanov,V.S., Gasilov,V.L. & Kazakov,Y.E. (2000) Features of electromagnetic radiation time-and-frequency fluctuation intensity distributions from human brain structures. *Critical Reviews in Biomedical Engineering* **28**, 160–182.

Latikka, J. & Eskola, H. (2018) The electrical conductivity of human cerebrospinal fluid *in vivo*. *IFMBE Proceedings* **67**, 773-776.

Latikka, J., Kuurne, T. A. & Eskola, H. (2001) Conductivity of living intracranial tissues. *Physics in Medicine and Biology* **46**, 1611.

Lonappan, A., Thomas, V., Bindu, G., Rajasekaran, C. & Mathew, K. T. (2006) Analysis of human cerebro spinal fluid at the ISM band of frequencies. *Journal of Electromagnetic Waves and Applications* **20**, 773–779.

Martin, B. & McElhaney, J. H. (1971) The acoustic properties of human skull bone. *Journal of Biomedical Materials Research* **5**, 325-333.

Mason, A., Goh, J. H., Korostynska, O., Al-Shamma'a, A., Field, M. & Browning, P. (2013) Real-time monitoring of bodily fluids using a novel electromagnetic wave sensor. *Brain Topography* **32**, 825-858.

McCann, H., Pisano, G. & Beltrachini, L. (2019) Variation in reported human head tissue electrical conductivity values. *Brain Topography* **32**, 825-858.

Mountcastle, V. (1957) Modality and topographic properties of single neurons of cat's somatic sensory cortex. *Journal of Neurophysiology* **20**, 408-434.

Noetscher, G., Htet, A. T., Elloian, J., Makarov, S. & Sciré-Scappuzzo, F. (2012) Detecting *in vivo* changes of electrical properties of cerebral spinal fluid using microwave signals from small coil antennas – numerical simulation. *IEEE Signal Processing in Medicine and Biology Symposium.*

Pethig, R. (1984) Dielectric Properties of biological materials: biophysical and medical applications. *IEEE Transactions on Electrical Insulation* EI-**19**, 453-474.

Sasaki, K, Wake, K. & Watanabe, S. (2014) Measurement of the dielectric properties of the epidermis and dermis at frequencies from 0.5 GHz to 110 GHz. *Physics in Medicine & Biology* **59**, 4739–4747.

Saxena, K., Singh, P., Sahoo, P., Sahu, S., Ghosh, S. et al. (2020) Fractal, scale free electromagnetic resonance of a single brain extracted microtubule nanowire, a single tubulin protein and a single neuron. *Fractal and Fractional* **4**, 1-16.

Scholkmann, F. (2015) Two emerging topics regarding long-range physical signaling in neurosystems: Membrane nanotubes and electromagnetic fields. *Journal of Integrative Neuroscience* **14***,* 717-733.

Sadleir, R. & Gabriel, C. (2021) *Electromagnetic Properties of Tissues. Electrical Impedance Tomography*. CRC Press, Boca Raton, FL.

Singh, P., Sarkar, J., Dey, P., Sarkar, S., Pattanaya, A., et. al. (2023) Inventing the potential of a high-frequency EEG, namely Dodecanogram (DDG): Human subjects' study. In, Kaiser, M.S., et al. (Eds) *Proceedings of the Fifth International Conference on Trends in Computational and Cognitive Engineering.* TCCE 2023. Lecture Notes in Networks and Systems, vol 961. Springer, Singapore.

Singh, P., Manna, J., Dey, P., Sarkar, S., Pattanayaka, A. et al. (2024) Dodecanogram (DDG): Advancing EEG technology with a high-frequency brain activity measurement device. *Journal of Multiscale Neuroscience* **3**, 13-26.

Tamura, T., Tenhunen,M. Lahtinen, T., Repo,T. & Schwan,H.P. (1994) Modelling of the dielectric properties of normal and irradiated skin. *Physics in Medicine and Biology* **39**, 927–936.

Tenti, G., Sivaloganathan, S. & Drake, J. (2002) The synchrony of arterial and CSF pulsations is not due to resonance. *Pediatric Neurosurgery* **37**, 221-222.

Tremblay, R., Lee, S. & Rudy, B. (2016) GABAergic Interneurons in the neocortex: from cellular properties to circuits. *Neuron* **91**, 260–292.

Vignes, J., Dagain, A., Guérin, J. & Liguoro, D. (2007) A hypothesis of cerebral venous system regulation based on a study of the junction between the cortical bridging veins and the superior sagittal sinus. *Journal of Neurosurgery* **107**, 1205-1210.

Walsh, D. R., Zhou, Z., Li, X., Kearns, J., Newport, D. & Mulvihill, J. (2020) Mechanical properties of the Cranial Meninges; A Systematic Review. *Journal of Neurotrauma* **38**, 1748-1761.

Wang, Shuya, LiuKun, WangYuan, WangShuyou, HeXun, Cui-xiang, GaoXinyan & ZhuBing (2017) A proposed neurologic pathway for scalp acupuncture: trigeminal nerve-meninges-cerebrospinal fluid-contacting neurons-brain. *Medical Acupuncture* **29**, 322–326.

Wang, Weice, Zhu, Mingxu, Liu, Benyuan, Li, Weichen, Wang, Yu, Li, Junyao, Guo, Qingdong, Du, Fang, Xu, Canhua & Shi, Xuetao (2024) Temperature and frequency dependence of human cerebrospinal fluid dielectric parameters. *Italian National Conference on Sensors* **22**, 7394.

Weise, K., Wartman, W., Knösche, T., Nummenmaa, A. & Makarov, S. (2022) The effect of meninges on the electric fields in TES and TMS. Numerical modeling with adaptive mesh refinement. *Brain Stimulation* **15**, 654-663.

Wells, R. (2005) *Cortical Neurons and Circuits: A Tutorial Introduction.* University of Idaho Library, Idaho.

White, D., Curry, G. R. & Stevenson, R. (1978) The acoustic characteristics of the skull. *Ultrasound in Medicine and Biology* **4**, 225-252.

Wiginton, J., Brazdzionis, J., Patchana, T., Hung, J., Zhang, Y., & Miulli, D. E. (2022) Novel method of electromagnetic field measurements of the human brain. *Cureus* **14**, e21982.

Zhou, Z. (2019) Evaluation of fluid-structure interaction and biofidelity of finite element head models. *Doctoral Thesis*, KTH Royal Institute of Technology, School of Engineering Science in Chemistry, Biotechnology and Health, Neuronic Engineering, SE-141 57 Huddinge, Sweden.